Research Square

Preprints are preliminary reports that have not undergone peer review.
They should not be considered conclusive, used to inform clinical practice,
or referenced by the media as validated information.

Mining-driven Forest Fragmentation Shapes Malaria Vector Ecology in the Venezuelan Amazon

Maria Eugenia Grillet

mariaeugenia.grillet@gmail.com

Universidad Central de Venezuela. Caracas

Abimel Moreno

Universidad Central de Venezuela. Caracas

Jorge E. Moreno

Servicio Autónomo Instituto de Altos Estudios Dr. Arnoldo Gabaldón MPPS

Sara A. Bickersmith

New York State Department of Health

Nelson Moncada

Universidad Central de Venezuela. Caracas

Victor Sanchez

Universidad Central de Venezuela. Caracas

Jan E. Conn

New York State Department of Health

Article

Keywords: Mosquito, Malaria, Mining, Forest, Amazon, Venezuela

Posted Date: November 20th, 2026

DOI: https://doi.org/10.21203/rs.3.rs-11446484/v1

License: This work is licensed under a Creative Commons Attribution 4.0 International License.
Read Full License

Additional Declarations: No competing interests reported.

Abstract

Malaria persistence in the Americas has paralleled rapid Amazonian deforestation, with Venezuela emerging as a critical hotspot where gold mining and forest loss drive intense epidemics. Because malaria transmission is tightly linked to mosquito ecology, clarifying how deforestation amplifies vector traits is essential. We examined forest fragmentation along mining gradients in the southern Venezuelan Amazon to assess impacts on anthropophilic anopheline mosquito communities. As expected, anopheline richness and abundance peaked at forest edges, particularly under intermediate fragmentation where edge effects were strongest, while mining pits further expanded populations. At broader scales, forest cover shaped species distributions, and long-degraded mining landscapes supported the greatest diversity and density of primary *Plasmodium* vectors, where malaria risk was particularly elevated during the dry-rainy transition. Vector mosquito assemblages were dominated by *Nyssorhynchus albitarsis* s.l. (*Ny. albitarsis* F, *Ny. janconnae*), *Ny. goeldii*, and *Ny. darlingi*. Notably, *Ny. janconnae* was reported for the first time in Venezuela and found infected with both *Plasmodium* species, while *Ny. rondoniensis*, also newly recorded, carried *P. falciparum*. These findings emphasize how escalating ecological pressures in the Amazon rainforest reshape vector composition, abundance, and infection dynamics, posing major challenges for malaria elimination in the region.

Introduction

Malaria remains a major public health challenge in the Amazon's humid tropical forest, which has consistently been the epicenter of transmission in the Americas over the past three decades. Between 2019 and 2024, Brazil and Venezuela alone reported nearly 3 million cases, around 80% of the continental total, with Venezuela as a critical hotspot[1,2]. Across the region, deforestation has emerged as the main environmental driver of persistent transmission and recurrent epidemics, with this pattern documented in Brazil[3,4], the Guianas[5], Peru[6,7], and Venezuela[8]. In Venezuela, the annual loss of 305 hectares of tree cover has been associated with a 0.7% rise in malaria incidence[8]. In Brazil, a 10% or 1% increase in deforestation has corresponded to malaria incidence increases ranging from 3.3%[9] to 6.3%[10], respectively. This overall pattern, conceptualized as "*frontier malaria*"[3], highlights both the consistency of the association and the variability in its magnitude across variable local contexts. It also emphasizes how forest degradation reshapes malaria epidemiology[11] and undermines control efforts across the Americas[12].

Despite extensive evidence linking land-use change to malaria reemergence, few studies have examined how mosquito vectors respond to the habitat disturbances caused by deforestation across the Amazon[12], even though their population dynamics are the central mechanism connecting deforestation to disease risk. Malaria transmission dynamics are primarily driven by vector traits, including feeding frequency, gonotrophic cycle length, abundance, and survival[13]. Elucidating how deforestation alters these life-history traits is critical to understanding the intensification of malaria in specific ecological settings.

In Venezuela, malaria transmission is predominantly localized in the southern state of Bolívar, where endemicity is strongly linked to the lowland rainforest ecosystems of the Venezuelan Amazon. Responsible for around 70% of all cases nationwide[14], this region continues to represent one of the highest-intensity *Plasmodium* hotspots in the Americas[2], notwithstanding the post-2019 decline following its major epidemic peak[1,8,15]. Here, gold mining exacerbates social vulnerability by increasing human exposure to vector biting, while associated deforestation sustains malaria transmission[8,16]. *Plasmodium vivax* predominates (72%), followed by *P. falciparum* (21%) and mixed infections (7%), with *Nyssorhynchus darlingi* and *Ny. albitarsis* s.l. as the main vectors, and *Ny. nuneztovari* s.l. implicated in *P. vivax* transmission[17,18]. Previous studies in this region have described the general habitat preferences of these species, noting their association with human settlements - whether mining, indigenous, or agricultural- situated along fragmented forest edges. They have also documented the use of natural breeding sites, such as river-pools, river-banks, forest and savanna lagoons, ponds and herbaceous swamps, as well as artificial habitats like mining-pits[17,19,20]. However, none have provided a quantitative assessment of how deforestation shapes vector ecology and consequently, transmission intensity, a gap the present study addresses. Assessing the feasibility of malaria elimination in Venezuela requires a clearer understanding of how mosquito populations respond to mining-driven deforestation in one of the Amazon's major hotspots.

This study analyzes spatial and temporal deforestation gradients across 38 mining sites in Sifontes municipality to evaluate how landscape structure influences anthropophilic *Anopheles* diversity, mosquito-human contact frequency, and *Plasmodium* infection rates. Building on ecological studies of Neotropical mosquito responses to forest disturbance[21,22], we hypothesize that intermediate levels of deforestation, where edge effects are strongest, will increase the abundance of anthropophilic anophelines, intensify human-mosquito contact, and elevate *Plasmodium* infection rates, particularly in forest-edge species such as *Ny. darlingi* and *Ny. albitarsis* s.l. Furthermore, based on prior studies[17], we expect that mining-driven land use change is expanding larval habitats for *Anopheles* vectors, thereby amplifying malaria risk as mining activities intensify.

Material and methods

Study area

Sifontes Municipality, Bolívar State, Venezuela, spans 25,560 km² along the Guyana-Brazil border and forms part of the Venezuelan Amazon (Fig. 1). Its ~ 58,000 residents are unevenly distributed across three parishes, with most in Tumeremo and smaller settlements extending south along Route 10 and river corridors (Dalla Costa and San Isidro). Northern savannahs contrast with southern lowland rainforests in these two parishes[23]. The climate is seasonal[24]: rains from May-August (peak June), dry season November-February, and transitional periods in March-April and September-October; mean annual temperatures are 24–26°C. Local livelihoods are dominated by illegal gold and diamond mining, which has driven deforestation and soil erosion for nearly three decades[16]. Environmental degradation

between 2001 and 2023 was marked by the loss of 39,000 ha of forest and an expansion of mining land from 14,797 to 34,465 ha[15,25]. In parallel, Venezuela recorded ~ 500,000 malaria cases from 2021 to 2024[2]; approximately 70% occurred in Bolívar State, where the Sifontes municipality alone contributed over half the disease burden. Infections with *P. vivax* and *P. falciparum* are strongly linked to mining occupations, mostly affecting males aged 15–40 years[8]. Primary vectors include *Nyssorhynchus darlingi* (formerly *Anopheles darlingi*), *Ny. albitarsis* s.l. (formerly *Anopheles albitarsis* s.l.), and *Ny. nuneztovari* s.l. (formerly *Anopheles nuneztovari* s.l.).

Studied localities

In Sifontes, housing ranges from permanent villages of rural populations and Amerindian groups (Pemón, Kariña) to provisional mining shelters concentrated in the southern parishes. Thirty-eight localities (Fig. 1) were selected for entomological and ecological analyses, based on mining history, malaria incidence, and accessibility. Populations ranged from 100-3,000 residents per locality, reporting 20 – 1,500 malaria cases during 2022-2025[14]. Housing is typically makeshift, with incomplete wooden or plastic walls, though localities vary considerably (see Supplementary Table S1 online).

Landscape analyses

Land-use maps (e.g., visualization) and landscape analyses (e.g., landscape metrics) were generated in the QGIS-free-software version 3.44 (Geographic Information System, https://qgis.org/). Classified raster images were obtained from the open Amazonian project, MapBiomas-Venezuela (https://mapbiomas.org/). Analyses were conducted at two spatial and temporal scales:

1. a) *Cluster-level temporal analysis and mining gradient*. Raster images were clipped using bounding polygons (“Extent”), and 5-km buffers around each locality were merged into 11 clusters. Mining cover was analyzed through time-series statistics for 2000, 2005, 2010, 2015, 2020, and 2024, with expansion trajectories (2000–2024) plotted (see Supplementary Figure S1 online) and acceleration rates estimated (see Supplementary Figure S2 online). Mining onset age correlated with mining cover ($r = 0.60$, $P < 0.001$), while forest loss increased with settlement age ($r = -0.40$, $P < 0.05$), indicating that expansion patterns capture deforestation dynamics. Based on these patterns, clusters were classified into four mining-age final groups reflecting forest modification over 0, 5, 10, and 25 years (Fig. 1, Supplementary Table S1 online): Group I (No Mining) showed no activity, Group II (Emerging) encompassed incipient areas with low coverage and slow growth (~ 5 years), Group III (Intensified) corresponded to rapidly expanding areas with exponential growth (~ 10 years), and Group IV (Established) represented long-standing areas with higher initial coverage and steady growth (~ 25 years).
2. b) *Local scale landscape metrics*. Landscape metrics were calculated within 2-km circular buffers centered on sampling points (Fig. 1). Metrics included mining cover (MC), forest cover (FC), forest edge length (FEL), and forest edge density (FED). MC and FC were extracted in hectares and

converted to percentages relative to the buffer area; FEL was measured in kilometers. Distances to mining water bodies (DMW), main roads (DMR), rivers, and forest edges (FE) were computed by converting raster layers to vector polygons and calculating shortest distances. The same polygonised layer was used to quantify the number of mining pits (NMP). FED was excluded from analyses due to near-perfect correlation with FEL (see Supplementary Figure S3 online). Additional land use areas, such as urban, were also estimated, and a land-cover map was generated for the study area (Fig. 1).

Entomological Sampling

From October 2022 to April 2025, adult female anophelines were collected using Human Landing Catch (HLC). Two trained collectors aspirated mosquitoes landing on human attractants between 18:00–24:00 h, covering peak vector activity[17,23]. Captures occurred prior to onset of blood feeding to reduce *Plasmodium* infection risk. At each locality, collections were conducted over two consecutive nights at peri-domestic (PD) sites and nearby forest edges (FE), with teams working simultaneously and ≥ 50 m apart. In total, 76 nights (38 localities × 2 nights) spanned both Rainy/Dry and Dry/Rainy transitions. PD sites were defined as one house per community (5–10 m from dwelling); FE sites were the nearest edge to the same house. Because PD-FE distances varied, this spatial relationship was treated as a study variable. Teams alternated between PD and FE to minimize bias. Mosquitoes were sorted by species, hour, site, day and locality, identified in the field using a morphological key[26], and preserved on silica gel at 4°C until DNA extraction.

Molecular methods: species identification and Plasmodium infection

We analyzed mosquito collections from preliminary sampling (2016–2017) and subsequent surveys (Oct-Nov 2022; Apr-May 2023) to confirm species identity and detect *Plasmodium* infections, following the sequential workflow outlined in Supplementary Figure S4 (online). Adult females collected in 2016–2017 are listed and described in Supplementary Table S2 (online), while those analyzed in 2022–2023 appear in Supplementary Table S3 (online).

Molecular species identification. Mosquitoes were identified using two complementary approaches: a) *ITS2-PCR-RFLP*: All specimens morphologically identified as anophelines or unknown species (N = 1367) were tested by PCR amplification of the internal transcribed spacer 2 (ITS2) region[27], followed by double-digest RFLP[28]; b) *COI* PCR and Sanger sequencing[29]: The cytochrome c oxidase subunit I (*COI*) barcode region was amplified for specimens identified by ITS2-PCR-RFLP as *Nyssorhynchus* (*Ny*.) *nuneztovari* s.l. or *Ny. albitarsis* s.l., to resolve species within these complexes. We included all samples from 2016–2017 and 2022, infected specimens from 2023, and individuals not resolved by ITS2-PCR-RFLP (see Supplementary Table S4 online). Raw sequences were cleaned, edited, screened for stop codons/pseudogenes, and queried against BLASTn using the software Geneious Prime version 2025.2.2 (https://www.geneious.com/).

Phylogenetic Analyses. COI sequences from the Nuneztovari and Albitarsis complexes were aligned with publicly available references using the molecular evolutionary genetic analysis software MEGA version 11 (https://www.megasoftware.net/). Unique haplotypes were identified with the online sequence toolbox FaBox version 1.61 (https://users-birc.au.dk/palle/php/fabox/). Bayesian inference (BI) analyses were performed in the online software for phylogeny, MrBayes, version 3.2.7 (https://www.phylogeny.fr/tools/mrbayes), applying the best-fit nucleotide substitution model selected by corrected Akaike Information Criterion in the bioinformatic software, jModeltest, version 2.1.10 (https://mybiosoftware.com/jmodeltest-phylogenetic-model-averaging.html#google_vignette). Consensus trees with posterior support were visualized in the online tool, Interactive Tree of Life (iTOL), version 7.4.2 (https://itol.embl.de/).

Plasmodium Detection. Mosquito samples were tested for *Plasmodium* infection (see Supplementary Table S4 and Supplementary Figure S4 online) using monoplex and triplex real-time PCR assays (StepOnePlus, ThermoFisher Scientific), following Bickersmith et al.[30]. Each assay was run in duplicate with the following controls: i) Negative control: water; ii) No-template control: gDNA from uninfected *Ny. darlingi*; iii) Positive controls: *P. falciparum*: 1,000× diluted MR4 MRA-149G (Genomic DNA, strain HB3-B2, BEI Resources, NIAID, NIH; contributed by Walliker et al.[31]); *Plasmodium vivax*: 1,000× diluted MR4 MRA-178 (Diagnostic plasmid containing 18S rRNA gene, BEI Resources, NIAID, NIH; contributed by Peter A. Zimmerman).

Data analysis

All analyses were conducted in the *R* free-software, version 4.4.4 (The *R*-Development Core Team, http://www.r-project.org). Two modeling approaches were used to assess landscape effects on anopheline abundance: regression trees (RTs) and generalized linear mixed models (GLMMs). RTs were built using (i) ANOVA trees with log-transformed abundances [log(abundance + 1)] and (ii) Poisson regression trees. Performance was compared by error rates and number of splits; for Poisson regression, equivalent error was achieved with 3- and 5-split trees, and the 3-split model was retained to reduce overfitting. Predictors included locality Group (proxy for mining), FC (%), DMW, FEL, NMP, and DFE. Despite high correlations (see Supplementary Figure S3 online), all were retained since RTs are less affected by multicollinearity. In the GLMMs models, to account for non-independence of data points arising from the sampling design (localities as experimental units and two sampling dates per locality), models were fitted with random intercepts for date and locality ID nested within date. Since each sampling date corresponded to unique localities, locality ID (comprising locality + site, with sites consistent across both dates) was nested within date. RTs identified locality Group as a strong predictor of abundance. GLMMs performed poorly with full datasets, likely due to sparsity, so models were stratified by locality group. Consequently, models were fitted using data subsets stratified by locality group according to species abundance patterns. Initially, full models included the following predictors: MC, DMW, DMR, FEL, and DFE. The FC and NMP variables were excluded due to strong correlations with MC (see Supplementary Figure S3 online) which would cause variance inflation in GLMMs. All predictors

were standardized before fitting, and simplification proceeded by sequential removal of non-significant terms. Final effects were expressed as incidence rate ratios (IRRs) from exponentiated estimates and 95% *CIs*.

Results

Landscape Ecology

Figure 1 illustrates the group of studied localities, highlighting contrasting regional-scale landscape features and local-scale characteristics from 2 km buffers around mosquito collection sites. Group IV localities exhibited the steepest and most sustained decline in forest cover, with markedly degraded forest structure (Table 1; Supplementary Figure S5) that peaked at intermediate forest cover (Supplementary Figure S6) as ecologically predicted. Groups II and III showed comparable fragmentation but diverging trajectories: Group III underwent sharp forest loss in the past decade, while Group II remained relatively stable over the last five years (Supplementary Figure S5). Group IV also contained more mining-generated water bodies or mining pits (Table 1; Supplementary Figure S5), typically within ~ 1 km of settlements. The most degraded forests were concentrated near the main road and rivers, forming a striking north-south gradient across the study area (Fig. 1; Table 1).

Table 1
Landscape metrics calculated within 2-km buffers around sampling localities in Sifontes Municipality, southern Venezuela. See main text for site grouping criteria. The metrics comprised mining cover, forest cover, forest edge length (FEL), distance to mining water bodies (DMW), distance to main roads (DMR), distance to near road (DNR), distance to main river (DMRiv), and number of mining pits (NMP)

Group	**Time variable**	**Landscape metrics (2 Km buffer)**							
Number of localities (N)	**Age of mining (Yr)**	**Forest cover (%) (μ ± SD)**	**Mining cover (%) (μ ± SD)**	**FEL (Km) (μ ± SE)**	**NMP (N) (μ ± SE)**	**DMW (Km) (μ ± SE)**	**DMRiv (Km) (μ ± SE)**	**DNR (Km) (μ ± SE)**	**DMR (Km) (μ ± SE)**
I (2)	**0**	**99**	**0**	**35 ± 3.0**	**0**	**32 ± 4.5**	**35 ± 8.5**	**0**	**40 ± 12.0**
II (12)	5	71 ± 23.3	12 ± 8.0	58 ± 5.1	3 ± 2.1	6 ± 2.7	10 ± 2.4	4 ± 2.0	20 ± 5.4
III (6)	10	75 ± 11.9	22 ± 15.8	61 ± 6.0	3 ± 2.1	2 ± 0.8	5 ± 1.1	4 ± 1.7	8 ± 1.1
IV (18)	25	57 ± 30.1	43 ± 29.7	72 ± 7.0	15 ± 4.6	1 ± 0.3	5 ± 0.7	2 ± 0.6	6 ± 1.1

Species composition and abundance

A total of 3,661 female anopheline mosquitoes were collected across all localities. Morphological identification revealed six species including 4 species complexes, which are presented here in order of occurrence: *Nyssorhynchus albitarsis* s.l. (n = 1794, 49%), *Ny. nuneztovari* s.l. (n = 988, 27%), *Ny. darlingi* (n = 732, 20%), *Ny. triannulatus* s.l. (n = 73, 2%), *Ny. oswaldoi* s.l. (n = 37, 1%), and *Ny. rondoniensis* (n = 37, 1%). Seasonal variation (Dry/Rainy vs. Rainy/Dry) and site-specific collections (FE vs. PD) significantly influenced anopheline abundance, with higher numbers observed during the Dry/Rainy season (Kruskal-Wallis, $H = 25.6$, $P < 0.001$) and at FE collection sites ($H = 22.4$, $P < 0.001$), compared to the Rainy/Dry season and PD collections (Fig. 2A). Molecular analyses enabled species resolution within the Albitarsis, Nuneztovari, and Oswaldoi complexes. Phylogenetic analysis further supported species delimitation within the Albitarsis and Nuneztovari complexes. Together, these analyses identified *Ny. albitarsis* F and *Ny. janconnae* (within the Albitarsis complex), *Ny. goeldii* (within the Nuneztovari complex), and *Ny. oswaldoi* B (within the Oswaldoi complex).

Species spatial distribution

Figure 2B illustrates the spatial distribution of the three most abundant *Nyssorhynchus* species across the regional landscape. High densities of *Ny. darlingi* were largely confined to the southern localities (Group IV), whereas *Ny. goeldii* was more frequently observed in Groups II and III. In contrast, *Ny. albitarsis* s.l. exhibited the broadest distribution, occurring across all localities. To explore the landscape factors shaping these patterns, we fitted Regression Tree models (RTMs) for *Ny. darlingi* and *Ny. albitarsis* s.l. The analysis (Fig. 3) revealed that mining age (MA), FC, and FEL jointly structured species occurrence, with MA and FC driving the dominant spatial patterns, while fragmentation amplified vector abundance along the mining-forest cover gradient. For *Ny. darlingi* (Fig. 3A), the RT's first split showed that mosquitoes were more abundant in older, heavily fragmented mining sites (Group IV) than in areas with little or no mining. The second split revealed that within Group IV, mosquito dominance was associated with sites having less than 84% FC and more than 73 km of FE, coinciding with a maximum degraded forest structure to intermediate vegetation cover (Supplementary Figure S6). In these localities, where the species was most frequently collected, mean FC was ~ 62% and mean FEL reached ~ 80 km. By comparison, the model for *Ny. albitarsis* s.l. (Fig. 3B) highlighted mining group classification as the strongest driver of distribution, while differences in FC fine-tuned the pattern at the local level. In this case, the species was most frequently collected in those sites where the mean FC was ~ 57% and mean FEL reached ~ 78 km. Limited data prevented RT modeling for *Ny. goeldii*.

To examine ecological relationships at the local scale, generalized linear mixed models (GLMMs) were further fitted for the three most abundant species. The best-fitting model for *Ny. darlingi* abundance incorporated three spatial environmental variables: distance to mining water body ($\chi2 = 7.14$, $df = 1$, $P = 0.008$), distance to the main road ($\chi2 = 18.67$, $df = 1$, $P < 0.001$), and distance to the forest edge ($\chi2 = 9.55$, $df = 1$, $P = 0.002$). The abundance of the species increased with closer proximity to each of these features (Fig. 4). For *Ny. albitarsis* s.l., the best model incorporated two spatial variables, distance to

mining water bodies ($\chi 2 = 10.43$, $df = 1$, $P = 0.001$) and distance to forest edge ($\chi 2 = 9.62$, $df = 1$, $P < 0.002$), along with land-use cover (mining) ($\chi 2 = 30.55$, $df = 1$, $P < 0.001$). Higher abundances of this species were associated with closer proximity to mining water (or mining pits) and FE, as well as greater mining area coverage (Fig. 5). Finally, the best model for *Ny. goeldi* included three spatial variables: distance to the main road ($\chi 2 = 16.79$, $df = 1$, $P < 0.001$), distance to the FE ($\chi 2 = 9.24$, $df = 1$, $P = 0.001$, and distance to mining water bodies ($\chi 2 = 5.81$, $df = 1$, $P = 0.05$). Abundance was greater in localities closer to FE and mining pits but farther from roads (Fig. 6).

Mosquito biting behavior and Plasmodium infections (569 words)

Analysis of mosquito biting activity revealed distinct temporal patterns across the three most abundant *Nyssorhynchus* species. By pooling data from collections across localities and collection sites over two sampling days, we could characterize their hourly biting behavior (Fig. 7A). Overall, human exposure to mosquito bites was consistently highest during the Dry/Rainy season, independent of collection site. A GLMM revealed a significant species effect on biting density ($X^2 = 15.94$, $df = 2$, $P < 0.001$). Specifically, *Ny. albitarsis* s.l. (including *Ny*. *albitarsis F* and *Ny*. *janconnae*) exhibited nearly fourfold higher biting rates compared to *Ny. darlingi* and *Ny. goeldii* (Fig. 7B). The latter two species did not differ significantly from one another, indicating comparable human exposure risk. *Nyssorhynchus darlingi* exhibited an almost continuous biting activity throughout the 6-hour nighttime sampling period, with a marked increase after 20:00 h, particularly in the Dry/Rainy season but showed an early biting peak (18:00) during the Rainy/Dry season. In contrast, *Ny. albitarsis* (including *Ny*. *albitarsis* F and *Ny*. *janconnae*) showed peak biting activity between 19:00–21:00 h in the Dry/Rainy season, with an earlier peak around 18:00–19:00 h in the Rainy/Dry season. Finally, *Ny. goeldii* bites were concentrated in the late afternoon and early evening (18:00–19:00 h).

Nightly and monthly entomological inoculation rates (*EIR*s) were estimated for *Nyssorhynchus* species testing positive for *Plasmodium* infections across 16 mining localities sampled during the Rainy/Dry season (2022) and the Dry/Rainy season (2023) (Table 2). A total of 69 infected mosquitoes were confirmed in 4 of the 16 localities: *Ny. darlingi* (n = 47), *Ny. albitarsis* s.l. (n = 13; 9 *Ny. albitarsis* F and 4 *Ny. janconnae*), and *Ny. rondoniensis* (n = 1). Most infections (74%) and consequently the highest *EIRs* were detected in PD collections from the MOR locality during the Dry/Rainy season, while the remaining 26% were identified in FE collections, both within MOR and other localities. Estimated exposure to mosquito bites for unprotected inhabitants ranged from 13.2 to 92.1 bites/person/night for *Ny. darlingi* and from 4.3 to 212.9 bites/person/night for *Ny. albitarsis* (= *Ny. albitarsis* F *and Ny. janconnae*). Elevated *P. falciparum* infection rates were detected exclusively in MOR for *Ny. darlingi*. In the same locality, *Ny. albitarsis* s.l. (one *Ny. albitarsis* F and two *Ny. janconnae*) also carried the parasite. For *Ny. darlingi*, the estimated *EIRs* were 10.7 infected bites/person with *P. vivax* and 6.4 with *P. falciparum*. Mixed infections (*P. vivax/P. falciparum*) were identified in two *Ny. darlingi* specimens (one from PD and one from FE collections), corresponding to 0.8 infective bites/person/night. Additionally, a single *Ny. rondoniensis* specimen was found infected with *P. falciparum* in the peridomestic area of MOR (April 2023), yielding an infection rate of 0.01 (1/88). In this locality, two specimens were collected over two nights, resulting in a

human biting rate (*HBR*) of 1 mosquito/person/night and corresponding nightly and monthly *EIRs* of 0.01 and 0.34, respectively. Of all the samples analyzed (N = 132) during the 2016–2017 sampling, two specimens of *Ny. albitarsis* F were positive for *P. vivax* from a locality called Mesones (MES) located in the region most degraded by mining in the south of the study area. Overall, the greatest risk of *Plasmodium* exposure and malaria transmission was associated with highly degraded forest landscapes from the established mining localities (Group IV). This coincided with the localities and region within the study area where the most malaria was reported during the study period (Supplementary Figure S5).

Table 2

Abundance, human bite rate (*HBR*), infection rates-IR (*Plasmodium*) in mosquitoes and entomological inoculation rates (*EIR*) of *Plasmodium* by *Ny. darlingi* and *Ny. albitarsis* (= F and *janconnae*) in 5 localities (2022, 2023), in southern Venezuela. N: total number of analyzed mosquitoes for parasite infection; IR: number of infected mosquitoes / totals analyzed; PV: *Plasmodium vivax*, PF: *P. falciparum* and PV + PF: *P. vivax*/*P. falciparum* mixed infection; *HBR*: geometric mean bites/person/night; monthly *HBR*: geometric mean bites/person/night x 30 days. *EIR*: *HBR* * IR

Locality	**Month - Year**	**Mosquito species**	**N**	***HBR* (95% CI) (Bite/person/ night)**	**IR (Infected /N)**		***EIR* (Infective bite/person/night & month)**		
Parasite species					**PV**	**PF**	**PV**	**PF**	**PV + PF**
PBE	Oct./Nov. 2022	*Ny. darlingi*	**29**	13.2 (7.8, 20.0)	0.03	0	0.4 / 12	0	0
PBE	Oct./Nov. 2022	*Ny. albitarsis* (*F*)	**8**	4.3 (1.9, 7.0)	0	0	0	0	0
GRA	Apr./May 2023	*Ny. darlingi*	**185**	92.1 (65.7, 27.1)	0.02	0	1.9 / 55	0	0
GRA	Apr./May 2023	*Ny. albitarsis* (F and *janconnae*)	**29**	9.8 (3.7, 18.1)	0	0	0	0	0
MOR	Apr./May 2023	*Ny. darlingi*	**181**	80.8 (55, 116.1)	0.13	0.08	10.7 / 315	6.4 / 194	0.01 (IR) 0.8 / 24
MOR	Apr./May 2023	*Ny. albitarsis* (F and *janconnae*)	**41**	18.1 (7.6, 33.5)	0.02	0.07	0.4 / 11	1.3 / 38	0
POR	Apr./May 2023	*Ny. darlingi*	**86**	37.8 (24.8, 55.1)	0.01	0	0.4 / 11	0	0
POR	Apr./May 2023	*Ny. albitarsis* (F and *janconnae*)	**467**	212.9 (159.7, 282.2)	0.01	0	2.1 / 64	0	0

Discussion

This study analyzed whether forest structure could predict vector diversity, abundance, and malaria risk in southern Venezuela's mining landscapes. As expected, models showed that anopheline richness and abundance were greatest at forest edges and at intermediate levels of forest fragmentation with mining pits (mining water bodies) further expanding anopheline populations. Along the mining gradient, long-established, highly degraded areas harbored the highest diversity and densities of the principal *Plasmodium* vectors. The community was dominated by the *Ny. albitarsis* complex (including *Ny. albitarsis* F and *Ny. janconnae*), *Ny. goeldii* (Nuneztovari complex) and *Ny. darlingi*, with rare records of *Ny. triannulatus* s.l., *Ny. oswaldoi* B (Oswaldoi complex), and *Ny. rondoniensis*. Spatial distributions of the dominant species reflected forest disturbance: *Ny. darlingi* concentrated in older degraded fields near roads and rivers, *Ny. albitarsis* was widespread across all sites, and *Ny. goeldii* favored younger, more forested zones. Malaria risk, especially from *P. falciparum* and mixed *P. falciparum*/*P. vivax* infections, peaked during the Dry/Rainy season and in the oldest degraded mining landscapes, as expected given the dominance of *Ny. darlingi*, *Ny. albitarsis* F and *Ny. janconnae*, with *Plasmodium* infections additionally detected in *Ny. rondoniensis*.

Our molecular findings expand Venezuela's malaria vector diversity and their South American range, confirming *Ny. albitarsis* F and *Ny. goeldii*, and newly detecting *Ny. janconnae* and *Ny. rondoniensis*. The Albitarsis Complex (*Ny. albitarsis* s.l.) currently comprises ten putative taxa[32,33], with *Ny. albitarsis* F and *Ny. albitarsis* I previously reported in Venezuela[20,34] and *Ny. janconnae*, previously described by Povoa et al.[35]. We also corroborated *Ny. goeldii* as a key member of the Nuneztovari Complex occurring in southern Venezuela, as it has been recently reported by Rubio et al.[36]. The Nuneztovari Complex (*Ny. nuneztovari* s.l.) includes four species: *Ny. nuneztovari* s.s., *Ny. jamariensis*, *Ny. goeldii*, and *Ny. dunhami*[37]. Importantly, *Ny. rondoniensis*, a recent species described within the Arthuri Complex, Strodei Subgroup in Brazil[38], is recorded here for the first time in Venezuela[39], adding a new species to the national inventory of anopheline richness. In addition, our findings highlight the sympatric distribution of sibling taxa within complexes (e.g., *Ny. albitarsis* F and *Ny. janconnae*) and accentuate the need for further molecular work in Sifontes to resolve species-specific ecological traits along the studied mining gradient.

At the local scale, both the diversity and abundance of anthropophilic anophelines were strongly structured by forest fragmentation, with our findings showing that proximity to forest edges is a significant predictor of *Ny. darlingi*, *Ny. albitarsis* s.l., and *Ny. goeldii* populations. The edge effect, the proliferation of ecotones at forest-matrix interfaces, consistently favors generalist species, as predicted by ecological theory[40]. *Nyssorhynchus darlingi*, in particular, has consistently been associated with forest edges across the Amazon, where females exploit edge vegetation as resting sites, while accessing nearby sources of blood and aquatic habitats for breeding[23,41,42]. Aquatic habitats near forest edges could accelerate larval development and potentially shorten the gonotrophic cycle of edge-adapted mosquitoes when blood sources are also readily available[12], reinforcing their dominance in human disturbed landscapes. Similar edge associations have been documented in Kenya, where survival of

female anophelines resting in humid forest-edge vegetation increased[43], highlighting how edge conditions enhance both reproduction and longevity of generalist vectors.

Beyond the edge effect, we observed that anopheline abundance peaked at intermediate disturbance levels, consistent with our hypothesis and with landscape ecology theory[40]. Forest fragmentation produces non-linear shifts in biodiversity, species turnover, and dominance, shaping the dynamics of forest-associated species. When forest cover is high (> 80%), edge density (the ratio of edge to interior habitat) is low and interior conditions prevail. When cover is very low (< 20%), few remnants remain and edge effects collapse. At intermediate forest cover (30–70%), edge length and patch heterogeneity peak, producing strong and large ecotones that favor generalist edge-species. This mechanism explains why *Ny. darlingi* in Brazil[22,42] and some mosquito species in Panama[21] reached maximum abundance under medium disturbance. Our findings extended this pattern to *Ny. albitarsis* s.l., emphasizing the ecological advantage of edge-adapted mosquitoes at these habitat interfaces.

Gold extraction by dredging in the Amazon removes sediments from deforested land, creating permanent pools that serve as breeding grounds for mosquitoes. The evidence presented here showed that the greater availability and proximity of these pools (mining-associated water bodies) near forests also predicted populations of *Ny. darlingi*, *Ny. albitarsis* s.l., and *Ny. goeldii*, corroborating our second hypothesis and reinforcing previous evidence that mining-driven aquatic habitats remain the most important vector breeding sites in this malaria hotspot[17,19,23]. In line with findings from Brazil and Peru[41,44], the most productive aquatic habitats for *Ny. darlingi* larvae are located near the edge of the forest where pre-adult stages develop under stable conditions, breeding mainly in large water bodies (e.g., lagoons, swamps, or riverbanks), where mixed light and vegetation sustain persistence[45]. Similarly, previous studies in Sifontes identified the preference of *Ny. albitarsis* s.l. and *Ny. goeldii* larvae for partially shaded sun-exposed lagoons and abundant aquatic vegetation[23], conditions typical of the sunlit lagoons left by miners in this area. The present study further demonstrated that *Ny. albitarsis* s.l. was strongly associated with mining land cover and mining water bodies along the gradient, accentuating its adaptation and population expansion in landscapes modified by mining. In summary, the convergence of edge proliferation, intermediate fragmentation, and mining-created habitats provides generalist anopheline vectors with a distinct ecological advantage in these disturbed forests of southern Venezuela.

Landscape structure can also influence the spatial distribution of mosquitoes through dispersal. Fragmentation and edge connectivity may facilitate movement, as shown for yellow fever vectors in the Atlantic Forest (Brazil), where edges and roads increased mosquito and virus spread and human contact[46], a mechanism scarcely examined for malaria vectors in the Amazon. Beyond forest configuration, we assessed adjacency to roads, rivers, urban settings, and other aquatic habitats. *Nyssorhynchus darlingi* was the only species associated with proximity to main roads and rivers, suggesting enhanced dispersal across ecosystem boundaries and toward alternative breeding sites, thereby linking this edge-forest mosquito to humans along settlement corridors. In the Amazon, *Ny.*

darlingi is often described as riverine but also shows strong associations with roads, both features shaping its distribution by connecting breeding sites to human populations. In southern Venezuela, its principal breeding sites occur along rivers, particularly in the western Amazon[47], with similar associations reported in Brazil[48] and Peru[41,49]. Road construction, such as the Iquitos-Nauta highway in Peru, has been linked to a 278-fold surge in *Ny. darlingi* biting rates and the creation of new larval habitats, highlighting how infrastructure development, often coupled with deforestation, can amplify malaria transmission risk by this edge-adapted species[41]. Similarly, in Peru, riverine communities where *Ny. darlingi* was present showed higher biting densities and, consequently, a 3.33-fold increase in *Plasmodium* transmission compared to other landscapes[49]. More recently, in Sifontes, Moreno et al.[23] reported that *Ny. darlingi* adults were 2.6 times more abundant along the road axis compared to collections from the mining area. These findings accentuate the adaptability of *Ny. darlingi* to diverse human-modified landscapes and the need for locally tailored approaches to understand its behavior.

Our results corroborated broader Amazonian evidence that deforestation and land-use change restructure anopheline communities, driving species turnover and shifts in dominant malaria vectors. At the landscape scale, *Ny. darlingi* and *Ny. albitarsis* s.l. dominated in old, fragmented mining environments, whereas *Ny. goeldii* remained tied to edges of relatively preserved forests, suggesting low adaptability to disturbance. The widespread distribution of *Ny. albitarsis* s.l. underlines its tolerance across disturbance gradients, particularly in mining-altered habitats, while *Ny. darlingi* concentrated in degraded mining areas and landscape corridors shaped by roads and rivers. Both species thus serve as sentinels of sustained human impact, albeit through distinct pathways.

In Sifontes, three decades of intense deforestation due to gold mining[16] have reshaped anopheline composition. Early surveys (1992–1997) reported low overall abundance, with *Ny. darlingi* most frequent[50]. Later studies (2000–2020) documented *Ny. albitarsis* s.l. overtaking *Ny. darlingi* as the principal vector, showing greater resilience to disturbance and rising infection rates[18,23,50]. *Nyssorhynchus nuneztovari* s.l. was first reported in 2003, despite intensive sampling since 1992, suggesting recent colonization[36]. Our findings confirm the predominance of *Ny. albitarsis* s.l. over *Ny. darlingi*, while also underlining the renewed relevance of *Ny. goeldii* in the more recent mining localities, and documenting new records in Sifontes, notably *Ny. rondoniensis*, seemingly favored by degraded mining habitats. Comparable species shifts have been observed elsewhere: *Ny. marajoara* replacing *Ny. darlingi* in Brazil[51]; dams and fish farms favoring generalists such as *Ny. darlingi*[22]; and *Ny. darlingi* re-invading the Peruvian Amazon in the 1990s, displacing *Ny. benarrochi* B, *Ny. oswaldoi* s.l., and *An. mattogrossensis*[41]. Together, these findings highlight the importance of predicting mosquito ecological responses to habitat fragmentation and other landscape-level changes, as these processes directly shape malaria risk, as we demonstrate below.

Miners faced the greatest peak exposure to anopheline bites during the Dry/Rainy season transition. Although biting rhythms varied slightly by species, the three dominant anthropophilic mosquitoes, *Ny. albitarsis* s.l., *Ny. goeldii*, and *Ny. darlingi*, concentrated activity in the late afternoon and early evening

(18:00–21:00 h), overlapping with outdoor human activity in PD areas. Estimated exposure for unprotected miners (*HBR*) reached over 200 or over 100 bites/person/night, primarily from *Ny. albitarsis* s.l. and *Ny. darlingi*, respectively. For *Ny. darlingi*, these *HBR*s exceeded previous reports from Venezuela (e.g., 10.5 bites/person/night in Moreno et al.[17]; 6.1 bites/person/night in Rubio-Palis et al.[52]) but were comparable to high-density records from French Guiana (e.g., Girod et al.[53]) and Brazil (e.g., Galardo et al.[54]). Similarly, high biting densities of *Ny. albitarsis* s.l. and *Ny. goeldii* have been reported in Brazil[55]. But methodological differences, geography, seasonality, taxonomic species resolution and local ecology warrant caution in comparing *HBR*s across Amazonian studies.

Crucially, the alignment of mosquito biting rhythms with human activity highlights periods of elevated outdoor transmission risk. This risk is compounded by miners living in precarious houses with incomplete walls, which allow greater mosquito entry and exposure, further undermining the effectiveness of long-lasting insecticidal nets (LLINs) in this Venezuelan hotspot. Across the Amazon, predominant vector life-history-traits (exophily, exophagy, and crepuscular feeding) limit the impact of LLINs, whose success depends partly on human behavior[56]. Ecological modifications also play a role: increased forest cover in Brazil[57] and deforestation in Peru[41,49] have been shown to modulate biting time or increase biting density of *Ny. darlingi*, respectively. Notably, *Ny. darlingi* exhibited later biting peaks in Sifontes two decades ago[17] compared to the earlier rhythms reported here, stressing the complex and dynamic interactions between mosquito ecology, behavior, forest disturbance and malaria risk.

High malaria transmission risk was concentrated in mining localities subjected to more than two decades of forest degradation, overlapping with areas that have historically sustained the highest malaria burden in Sifontes municipality[8], Venezuela[14], and the Americas[2]. Approximately 68% of *Plasmodium*-infected mosquitoes were *Ny. darlingi*, harboring *P. vivax*, *P. falciparum*, and mixed infections. This reinforces the central role of *Ny. darlingi* as the primary malaria vector in the region[56] and highlights the exceptionally high transmission intensity associated with degraded mining landscapes[8]. Exposure estimates indicate that an unprotected miner could receive nightly doses of approximately 11 infective bites carrying *P. vivax*, 6 carrying *P. falciparum*, and up to 1 mixed infection. These estimates greatly exceed those reported by Moreno et al.[19] for the same mining localities (2.21 infective bites/person/night for *Ny. darlingi*), suggesting a marked escalation of malaria transmission over time in the region.

By contrast, although *Ny. albitarsis* s.l. was the dominant biting species, it accounted for only about one-third of *Plasmodium* infections. Both *Ny. albitarsis* F and *Ny. janconnae* were found infected with *P. vivax* and *P. falciparum*, showing their complementary role in sustaining transmission alongside *Ny. darlingi*. Importantly, this study provides the first evidence of *P. vivax* and *P. falciparum* infections in *Ny. janconnae* within the Venezuelan Amazon, expanding the national and regional vector profile for this species complex. Exposure estimates suggest miners could receive about one infective bite per night from *Ny. albitarsis* s.l. Contrary to the suggestion by Abou et al.[18] that *Ny. albitarsis* s.l. may be more efficient than *Ny. darlingi* in Sifontes municipality, our results align with expectations of *Ny. darlingi* as the primary

regional vector. Future analyses along the mining gradient should clarify the relative contribution and efficiency of each sibling species of *Ny. albitarsis* s.l., as current evidence indicates they likely play comparable roles.

Spatially, 74% of infections were recorded in PD collections, highlighting intense human-vector contact near households, while 26% occurred at FE, confirming that transmission risk extends beyond PD environments in these mining localities. Temporally, the highest risk coincided with the transition between Dry and Rainy seasons. If *Ny. darlingi* and *Ny. albitarsis* s.l. populations indeed survive longer during this period, as our data suggest, their vectorial capacity would increase, reinforcing seasonal peaks in transmission, a pattern consistent with findings from Brazil[55]. Future studies in Sifontes should address this hypothesis.

A gap in the present results lies in the vector role of *Ny. goeldii*, whose abundance was lower in the highly degraded mining sites. Previously, in the municipality of Sifontes, *Ny. goeldii* (as Nuneztovari) has been found infected with *P. vivax*[18]. Subsequent analyses along the studied gradient where this species is more abundant could aim to evaluate its possible contribution to the transmission of *P. falciparum*. Finally, we detected *P. falciparum* infection in a single *Ny. rondoniensis* mosquito from Morrocoy, the locality with the highest concentration of *Plasmodium* infections. Although rare (infection rate 0.01), its presence in peridomestic areas suggests that secondary vectors may contribute to residual transmission under specific ecological conditions. This expands the list of potential local vectors and highlights the need for surveillance of emerging species of epidemiological relevance in southern Venezuela.

Limitation of the study

The results presented here are based on approximately 912 hours of field sampling across 38 sites spanning both Rainy-to-Dry and Dry-to-Rainy transitions in the Venezuelan Amazon. Despite the substantial number of specimens collected and analyzed - representing each of the four mining landscape categories studied - numbers of *Ny. albitarsis* s.l. and *Ny. goeldii* successfully sequenced were relatively small compared with the total collection of these two species complexes. As our primary objective was to characterize the ecology of these species along the forest fragmentation gradient, species delimitation within complexes and the detection of *Plasmodium*-infected mosquitoes were therefore concentrated in the locations with the greatest diversity and abundance: long-degraded mining areas (Group IV localities). At present, additional specimens are being sequenced to expand coverage across the other locality groups (I, II, and III), efforts will allow us to corroborate the distribution of *Ny. albitarsis* F, *Ny. janconnae*, and *Ny. goeldii*, as well as their species-specific ecology, and finally to clarify their role as *Plasmodium* vectors in these settings, thereby strengthening the generalizability of our findings.

Conclusions

Our results demonstrate that *Plasmodium*-infected mosquitoes are concentrated in fragmented landscapes with high edge density and intermediate forest cover, highlighting how deforestation can amplify malaria transmission through nonlinear ecological mechanisms[12]. The consistency of this pattern with findings from the Brazilian Amazon[4,58] suggests a broader regional process operating across Amazonian frontiers. In southern Venezuela, where gold-mining expansion has dramatically accelerated forest loss[15], these landscape transformations have sustained resilient *P. vivax* and *P. falciparum* hotspots for decades[8]. By acting as persistent sources of infection that re-establish transmission after local declines, such hotspots represent a major barrier to elimination efforts across the Americas.

These findings underline that malaria elimination cannot be achieved through vector control and case management alone. Because landscape change directly influences the ecological conditions that sustain transmission, environmental degradation must be recognized as a central determinant of malaria risk. Integrating landscape monitoring into surveillance systems and intervention planning will be essential for targeting emerging hotspots and preventing transmission resurgence. Ultimately, a One Health approach that explicitly incorporates land-use change, ecosystem integrity, and human health is critical for achieving long-term malaria elimination in the region.

Data availability

Sequence data supporting this study's findings and the unique COI haplotypes sequences to identify mosquito species molecularly have been deposited in GenBank repository (Accession ids: QB175542-QB175610). Entomological and ecological data are available at: (https://github.com/AbimelMoreno/grilletetal_2026).

Declarations

Data availability

Sequence data supporting this study's findings and the unique COI haplotypes sequences to identify mosquito species molecularly have been deposited in GenBank repository (Accession ids: QB175542-QB175610). Entomological and ecological data are available at: (https://github.com/AbimelMoreno/grilletetal_2026).

Acknowledgments

We gratefully acknowledge the logistical support provided by Luis Petterson, William Anaya Rincón, Beatriz González, and Ralfina González. We also extend our thanks to the *Consejo de Desarrollo Científico y Humanístico*, Universidad Central de Venezuela (CDCH-UCV), and in particular to Félix Tapia, Darling Ojeda, Ana Bonilla, Yadira Rangel, Ruth Rodríguez, Lissette Rangel and María Rodríguez, for their dedicated administrative assistance. We would like to thank the Wadsworth Center Advanced Genomic

Technologies Core (New York State Department of Health, Albany, NY) for the Sanger sequencing contributions.

Author Contributions

MEG: Conceptualization, Methodology, Formal analysis, Validation, Investigation, Project administration, Supervision, Writing – original draft, Writing – final review & editing. AM: Data curation, Formal analysis, Visualization, Writing – review & editing; JEM: Methodology, Investigation, Supervision, Writing – review & editing; SB: Formal analysis, Visualization, Writing – review & editing; NM: Methodology, Writing – review & editing; VS: Methodology, Writing – review; JEC: Conceptualization, Investigation, Funding acquisition, Writing – review & editing. All authors reviewed, edited and approved the final manuscript

Funding

This work was supported by the U.S. National Institutes of Health (grant R01 AI110112) to JEC.

Declarations

Declaration of AI-Assisted Technologies in the Writing Process

MEG used Microsoft Copilot (accessed October 2026) solely to assist with grammar and style. This process enhanced clarity and coherence while preserving the authors' original ideas. The manuscript was subsequently reviewed and revised by the authors, who take full responsibility for its content.

Competing Interests: The authors declare no competing interests

Ethics approval and consent to participate

The study was approved by the ethics committee (the National Bioethics Center of Venezuela, CIBI-CENABI) of Central University of Venezuela. For Human Landing Catches, procedures, benefits, and risks were explained to collectors, and informed consent was obtained. Collectors were monitored for malaria after each sampling period using standard rapid diagnostic tests. All entomological procedures followed relevant guidelines and regulations.

Consent for publication

Not applicable.

Additional Information

Supplementary information

Available online

References

1. Grillet, M. E. et al. Venezuela's humanitarian crisis, resurgence of vector-borne diseases, and implications for spillover in the region. *Lancet Infect. Dis.* **19**, e149–e161. https://doi.org/10.1016/S1473-3099(18)30757-6 (2019).
2. World Health Organization. *World malaria report 2025: addressing the threat of antimalarial drug resistance. 213* (Geneva, 2025).
3. Castro, M. C., Monte-Mor, R. L., Sawyer, D. O. & Singer, B. H. Malaria risk on the Amazon frontier. *Proc. Natl. Acad. Sci. U. S. A.* 103, 2452–2457. (2006). https://doi.org/10.1073/pnas.0510576103
4. Laporta, G. Z. et al. Malaria transmission in landscapes with varying deforestation levels and timelines in the Amazon: a longitudinal spatiotemporal study. *Sci. Rep.* **11**, 6477. https://doi.org/10.1038/s41598-021-85890-3 (2021).
5. Douine, M. et al. Malaria in gold miners in the Guianas and the Amazon: Current knowledge and challenges. *Curr. Trop. Med. Rep.* **7**, 37–47. https://doi.org/10.1007/s40475-020-00202-5 (2020).
6. Sanchez, J. F. et al. Unstable malaria transmission in the Southern Peruvian Amazon and its association with gold mining, Madre de Dios, 2001–2012. *Am. J. Trop. Med. Hyg.* **96**, 304–311. https://doi.org/10.4269/ajtmh.16-0030 (2017).
7. Aguirre, J., Rojas, P., Yu, T. E. & Yenerall, J. Spatial spillovers and the relationship between deforestation and malaria: evidence from the Peruvian Amazon. *J. Environ. Plan. Manag*. 1–17. https://doi.org/10.1080/09640568.2023.2289102 (2024).
8. Grillet, M. E. et al. Malaria in Southern Venezuela: The hottest hotspot in Latin America. *PLoS Negl. Trop. Dis.* **15**, e0008211. https://doi.org/10.1371/journal.pntd.0008211 (2021).
9. MacDonald, A. J. & Mordecai, E. A. Amazon deforestation drives malaria transmission, and malaria burden reduces forest clearing. *Proc. Natl. Acad. Sci. U. S. A.* 116, 22212–22218. (2019). https://doi.org/10.1073/pnas.1905315116
10. Arisco, N. J., Peterka, C., Diniz, C., Singer, B. H. & Castro, M. C. Ecological change increases malaria risk in the Brazilian Amazon. *Proc. Natl. Acad. Sci. U. S. A.* 121, e2409583121. (2024). https://doi.org/10.1073/pnas.2409583121
11. Fornace, K. M., Diaz, A. V., Lines, J. & Drakeley, C. J. Achieving global malaria eradication in changing landscapes. *Malar. J.* **20**, 69. https://doi.org/10.1186/s12936-021-03599-0 (2021).
12. Grillet, M. E., Sallum, M. A. M. & Conn, J. E. Deforestation, mosquito ecology, and malaria elimination in the Amazon Region. *Annu. Rev. Entomol.* **71**, 497–517. https://doi.org/10.1146/annurev-ento-030625-035915 (2026).
13. Garrett-Jones, C. Prognosis for interruption of malaria transmission through assessment of the mosquito's vectorial capacity. *Nature* **204**, 1173–1175 (1964).
14. Ministerio del Poder Popular para la Salud (MPPS). Boletín Epidemiológico - Semana Epidemiológica Nº37, 13 al 19 de septiembre de 2026. (2026). https://mpps.gob.ve/boletines-epidemiologicos/
15. Grillet, M. E., Moreno, J. E., Paníz-Mondolfi, A. & Navarro, J. C. in *Planetary health approaches to understand and control vector-borne diseases* Vol. 8 *Ecology and control of vector-borne diseases* Ch.

2, 34–53Wageningen Academic, (2024).

16. Fletcher, I. K. et al. Synergies between environmental degradation and climate variation on malaria re-emergence in southern Venezuela: a spatiotemporal modelling study. *Lancet Planet. Health*. **6**, e739–e748. https://doi.org/10.1016/S2542-5196(22)00192-9 (2022).
17. Moreno, J. E., Rubio-Palis, Y., Paez, E., Perez, E. & Sanchez, V. Abundance, biting behaviour and parous rate of anopheline mosquito species in relation to malaria incidence in gold-mining areas of southern Venezuela. *Med. Vet. Entomol.* **21**, 339–349. https://doi.org/10.1111/j.1365-2915.2007.00704.x (2007).
18. Abou Orm, S., Moreno, J. E., Carrozza, M., Acevedo, P. & Herrera, F. *Plasmodium spp*. infection rates for some *Anopheles spp*. from Sifontes Municipality, Bolívar State, Venezuela. *Bol. Malariol. Salud Ambient.* LVII, 17–25 (2017).
19. Moreno, J. E. et al. Malaria entomological inoculation rates in gold mining areas of Southern Venezuela. *Mem. Inst. Oswaldo Cruz*. **104**, 764–768. https://doi.org/10.1590/s0074-02762009000500017 (2009).
20. Zúñiga, M. A., Rubio-Palis, Y. & Brochero, H. Updating the bionomy and geographical distribution of *Anopheles (Nyssorhynchus) albitarsis* F: A vector of malaria parasites in northern South America. *PLoS One*. **16**, e0253230. https://doi.org/10.1371/journal.pone.0253230 (2021).
21. Loaiza, J. R. et al. Disturbance and mosquito diversity in the lowland tropical rainforest of central Panama. *Sci. Rep.* **7**, 7248. https://doi.org/10.1038/s41598-017-07476-2 (2017).
22. Chaves, L. S. M. et al. Anthropogenic landscape decreases mosquito biodiversity and drives malaria vector proliferation in the Amazon rainforest. *PLoS One*. **16**, e0245087. https://doi.org/10.1371/journal.pone.0245087 (2021).
23. Moreno, J. E., Domínguez, C., Molina, D., Sanchez, V. & Amaya, W. Establecimiento de una línea de base entomológica de malaria en la parroquia San Isidro del municipio Sifontes del estado Bolívar, Venezuela [Establishment of an entomological malaria baseline in the San Isidro parish of the Sifontes municipality of Bolívar state, Venezuela]. *Bol. Malariol. Salud Ambient*. **60**, 101–108 (2020).
24. Grillet, M. E., Souki, E., Laguna, M., Leon, J. R. & F. & The periodicity of *Plasmodium vivax* and *Plasmodium falciparum* in Venezuela. *Acta Trop.* **129**, 52–60. https://doi.org/10.1016/j.actatropica.2013.10.007 (2014).
25. Hansen, M. C. et al. High-resolution global maps of 21st-Century forest cover change. *Science* **342**, 850–853. https://doi.org/10.1126/science.1244693 (2013).
26. Faran, M. E. & Linthicum, K. J. A handbook of the Amazonian species of *Anopheles (Nyssorhynchus)* (Diptera: Culicidae). *Mosq. Syst.* **13**, 1–81 (1981).
27. Marrelli, M. T. et al. Amazonian malaria vector anopheline relationships interpreted from ITS2 rDNA sequences. *Med. Vet. Entomol.* **19**, 208–218. https://doi.org/10.1111/j.0269-283X.2005.00558.x (2005).
28. Matson, R. et al. Improved molecular technique for the differentiation of neotropical anopheline species. *Am. J. Trop. Med. Hyg.* **78**, 492–498 (2008).

29. Folmer, O., Black, M., Hoeh, W., Lutz, R. & Vrijenhoek, R. DNA primers for amplification of mitochondrial cytochrome c oxidase subunit I from diverse metazoan invertebrates. *Mol. Mar. Biol. Biotechnol.* **3**, 294–299 (1994).
30. Bickersmith, S. A. et al. A sensitive, specific and reproducible real-time PCR method for detection of *Plasmodium vivax* and *Plasmodium falciparum* infection in field-collected anophelines. *Mem. Inst. Oswaldo Cruz*. **110**, 573–576. https://doi.org/10.1590/0074-02760150031 (2015).
31. Walliker, D. et al. Genetic analysis of the human malaria parasite *Plasmodium falciparum*. *Science* **236**, 1661–1666. https://doi.org/10.1126/science.3299700 (1987).
32. Bourke, B. P. et al. Phylogenetic analysis of the Neotropical Albitarsis Complex based on mitogenome data. *Parasit. Vectors*. **14**, 589. https://doi.org/10.1186/s13071-021-05090-w (2021).
33. Motoki, M. T., Linton, Y. M., Conn, J. E., Ruiz-Lopez, F. & Wilkerson, R. C. Phylogenetic network of mitochondrial COI gene sequences distinguishes 10 taxa within the Neotropical Albitarsis Group (Diptera: Culicidae), confirming the separate species status of *Anopheles albitarsis* H (Diptera: Culicidae) and revealing a novel lineage, *Anopheles albitarsis* J. *J. Med. Entomol.* **58**, 599–607. https://doi.org/10.1093/jme/tjaa211 (2021).
34. Ruiz-Lopez, F. et al. DNA barcoding reveals both known and novel taxa in the Albitarsis Group (*Anopheles: Nyssorhynchus*) of Neotropical malaria vectors. *Parasit. Vectors*. **5**, 44. https://doi.org/10.1186/1756-3305-5-44 (2012).
35. Povoa, M. M. et al. The importance of *Anopheles albitarsis* E and *An. darlingi* in human malaria transmission in Boa Vista, state of Roraima, Brazil. *Mem. Inst. Oswaldo Cruz*. **101**, 163–168. https://doi.org/10.1590/s0074-02762006000200008 (2006).
36. Rubio-Palis, Y., Corredor-Medina, C. & Lenhart, A. E. Ruiz-López, F. *Anopheles* species complexes from Guyana and Venezuela malaria endemic areas using COI sequences. *Malar. J.* https://doi.org/10.1186/s12936-026-05791-6 (2026).
37. Sant'Ana, D. C. & Sallum, M. A. M. A new species of the Nuneztovari Complex of *Nyssorhynchus* (Diptera: Culicidae) from the western Brazilian Amazon. *Zootaxa* **5134**, 275–285. https://doi.org/10.11646/zootaxa.5134.2.6 (2022).
38. Sant'Ana, D. C. & Sallum, M. A. M. A new species of the Arthuri Complex of the Strodei Subgroup of *Nyssorhynchus* (Diptera: Culicidae). *Zootaxa* **5175**, 559–569. https://doi.org/10.11646/zootaxa.5175.5.5 (2022).
39. Conn, J. E. et al. First detection of *Nyssorhynchus rondoniensis* (Diptera: Culicidae) in southern Venezuela and its infection with *Plasmodium falciparum*. *Acta Trop.* **270**, 107802. https://doi.org/10.1016/j.actatropica.2025.107802 (2025).
40. Fahrig, L. Effects of habitat fragmentation on biodiversity. *Annu. Rev. Ecol. Evol. Syst.* **34**, 487–515. https://doi.org/10.1146/annurev.ecolsys.34.011802.132419 (2003).
41. Vittor, A. Y. et al. Linking deforestation to malaria in the Amazon: Characterization of the breeding habitat of the principal malaria vector, *Anopheles darlingi*. *Am. J. Trop. Med. Hyg.* **81**, 5–12 (2009).

42. Barros, F. S. & Honorio, N. A. Deforestation and malaria on the Amazon Frontier: Larval clustering of *Anopheles darlingi* (Diptera: Culicidae) determines focal distribution of malaria. *Am. J. Trop. Med. Hyg.* **93**, 939–953. https://doi.org/10.4269/ajtmh.15-0042 (2015).
43. Kweka, E. J., Kimaro, E. E. & Munga, S. Effect of deforestation and land use changes on mosquito productivity and development in Western Kenya Highlands: Implication for malaria risk. *Front. Public. Health*. **4**, 238. https://doi.org/10.3389/fpubh.2016.00238 (2016).
44. Singer, B. H. & de Castro, M. C. Agricultural colonization and malaria on the Amazon frontier. *Ann. N Y Acad. Sci.* **954**, 184–222. https://doi.org/10.1111/j.1749-6632.2001.tb02753.x (2001).
45. Hiwat, H. & Bretas, G. Ecology of *Anopheles darlingi* Root with respect to vector importance: a review. *Parasit. Vectors*. **4**, 177. https://doi.org/10.1186/1756-3305-4-177 (2011).
46. Prist, P. R. et al. Roads and forest edges facilitate yellow fever virus dispersion. *J. Appl. Ecol.* **59**, 4–17. https://doi.org/10.1111/1365-2664.14031 (2022).
47. Magris, M., Rubio-Palis, Y., Menares, C. & Villegas, L. Vector bionomics and malaria transmission in the Upper Orinoco River, Southern Venezuela. *Mem. Inst. Oswaldo Cruz*. **102**, 303–311. https://doi.org/10.1590/s0074-02762007005000049 (2007).
48. Gil, L. H., Tada, M. S., Katsuragawa, T. H., Ribolla, P. E. & da Silva, L. H. Urban and suburban malaria in Rondonia (Brazilian Western Amazon) II. Perennial transmissions with high anopheline densities are associated with human environmental changes. *Mem. Inst. Oswaldo Cruz*. **102**, 271–276. https://doi.org/10.1590/s0074-02762007005000013 (2007).
49. Lainhart, W. et al. Evidence for temporal population replacement and the signature of ecological adaptation in a major Neotropical malaria vector in Amazonian Peru. *Malar. J.* **14**, 375. https://doi.org/10.1186/s12936-015-0863-4 (2015).
50. Moreno, J. E., Rubio-Palis, Y., Sanchez, V. & Mariany, D. [Primer registro de *Anopheles (Nyssorhynchus) nuneztovari* Gabaldón,1940 (Diptera: Culicidae) en el estado Bolívar, Venezuela y sus implicaciones eco-epidemiológicas]. *Entomotropica* **19**, 55–58 (2004).
51. Conn, J. E. et al. Emergence of a new neotropical malaria vector facilitated by human migration and changes in land use. *Am. J. Trop. Med. Hyg.* **66**, 18–22. https://doi.org/10.4269/ajtmh.2002.66.18 (2002).
52. Rubio-Palis, Y. et al. Malaria entomological risk factors in relation to land cover in the Lower Caura River Basin, Venezuela. *Mem. Inst. Oswaldo Cruz*. **108**, 220–228. https://doi.org/10.1590/0074-0276108022013015 (2013).
53. Girod, R., Gaborit, P., Carinci, R., Issaly, J. & Fouque, F. *Anopheles darlingi* bionomics and transmission of *Plasmodium falciparum, Plasmodium vivax* and *Plasmodium malariae* in Amerindian villages of the Upper-Maroni Amazonian forest, French Guiana. *Mem. Inst. Oswaldo Cruz*. **103**, 702–710. https://doi.org/10.1590/s0074-02762008000700013 (2008).
54. Galardo, A. K. et al. Malaria vector incrimination in three rural riverine villages in the Brazilian Amazon. *Am. J. Trop. Med. Hyg.* **76**, 461–469 (2007).

55. Zimmerman, R. H. et al. Vectorial capacities for malaria in eastern Amazonian Brazil depend on village, vector species, season, and parasite species. *Malar. J.* **21**, 237. https://doi.org/10.1186/s12936-022-04255-x (2022).
56. Conn, J. E., Sallum, M., Correa, M. M. & Grillet, M. E. in *in Towards Malaria Elimination - A Leap Forward*. 281–313 (eds Manguin, S. & Dev, V.) (Intech Open, 2018).
57. Chaves, L. S. M. et al. Forest cover percentage drives the peak biting time of *Nyssorhynchus darlingi* (Diptera: Culicidae) in the Brazilian Amazon. *Malar. J.* **23**, 166. https://doi.org/10.1186/s12936-024-04984-1 (2024).
58. Chaves, L. S. M., Conn, J. E., López, R. V. M. & Sallum, M. A. M. Abundance of impacted forest patches less than 5 km^2 is a key driver of the incidence of malaria in Amazonian Brazil. *Sci. Rep.* **8**, 7077. https://doi.org/10.1038/s41598-018-25344-5 (2018).

Figures

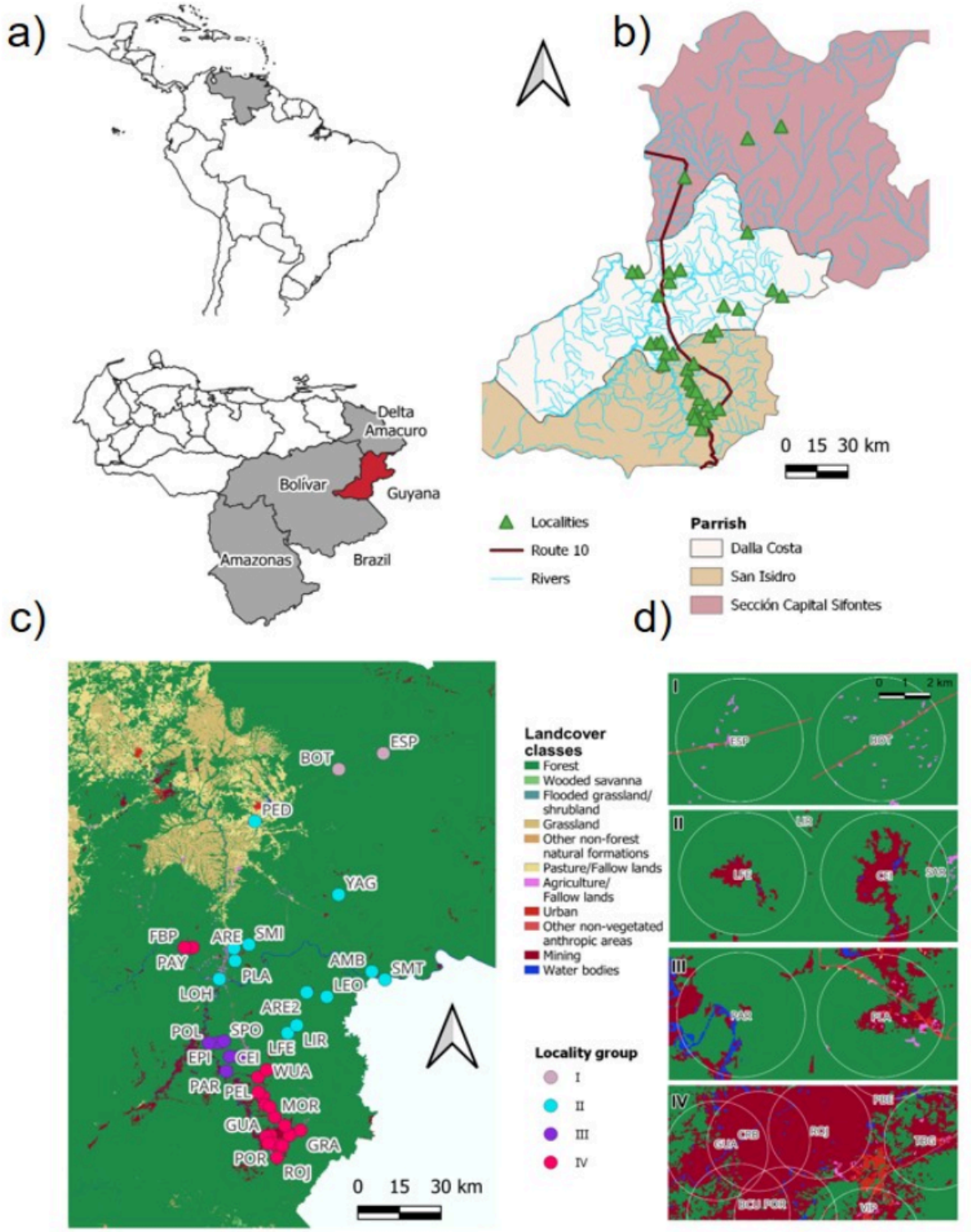


Figure 1

Map of South America and Venezuela (A) highlighting Amazonian states (light grey shading) and the location of Sifontes Municipality (red). Studied mining localities (green symbols) correspond to mosquito collection sites within Sifontes (B). Land-use map of the study area (C) derived from raster images provided by the Amazonian project MapBiomas-Venezuela (https://venezuela.mapbiomas.org/).

Examples of 2-km circular buffers centered on sampling points illustrating mining-age groups of localities and representing a deforestation timeline from which landscape metrics were calculated (D).

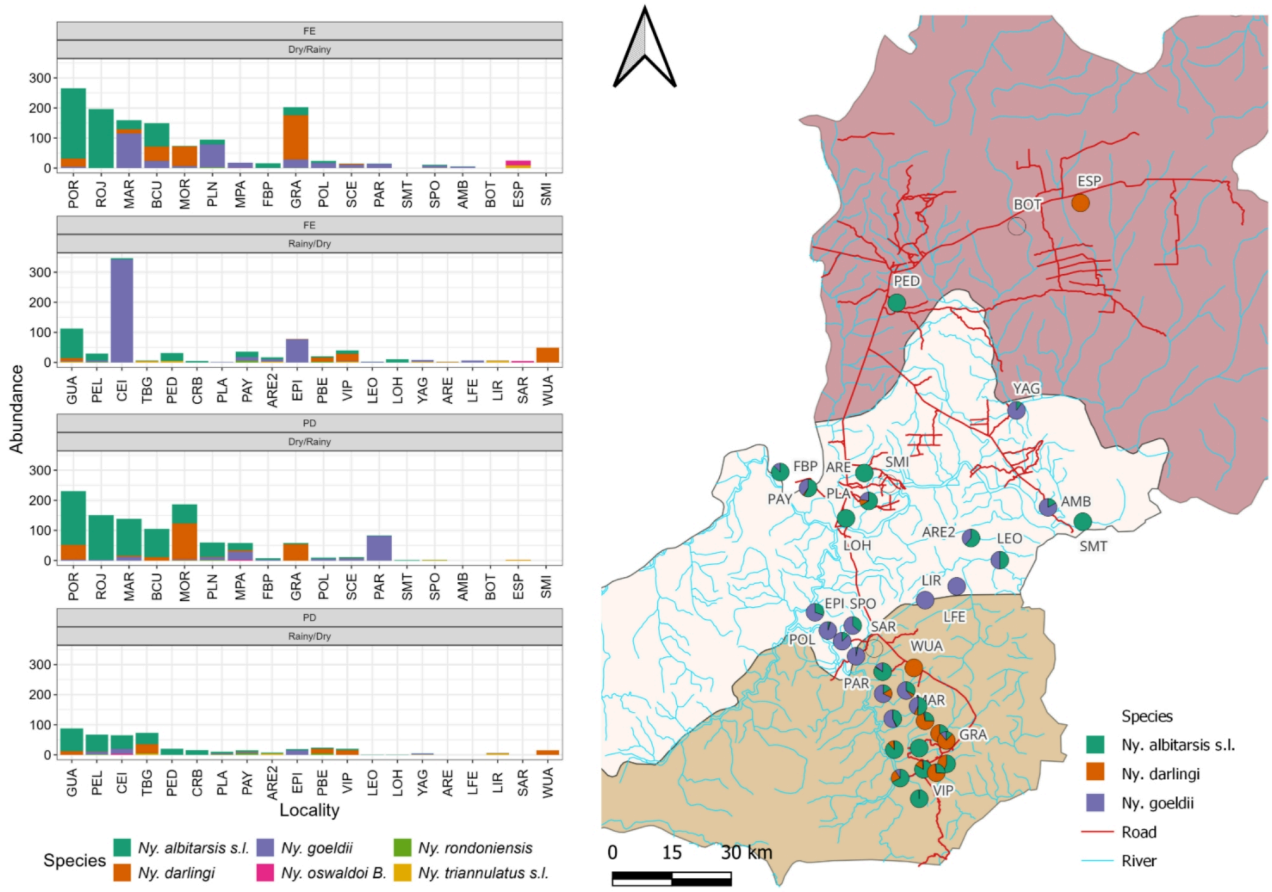


Figure 2

(A) Abundance (total number) of the six *Nyssorhynchus* species across localities (see SupplementaryTable S1 online for locality codes), seasons, and collection sites (PD, FE). Sampling periods: Dry/Rainy (April/May 2023 and 2024, April 2025) and Rainy/Dry (Oct/Nov 2022, Sept/Oct 2023, Nov 2024) seasons. **(B)** Proportion (%) and spatial distribution of *Ny. albitarsis* s.l., *Ny. darlingi*, and *Ny. goeldii* across the 38 sampled localities in Sifontes Municipality.

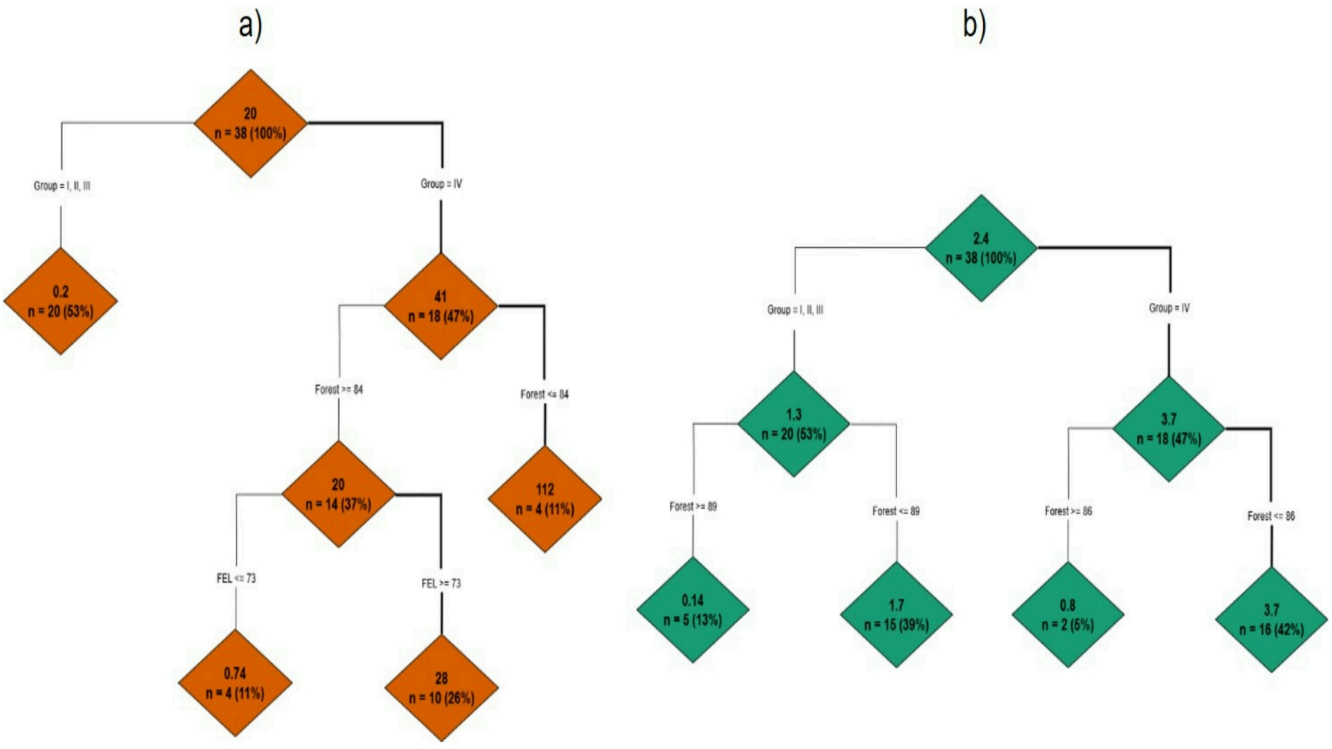


Figure 3

Regression trees illustrating the effects of mining age (Group), forest cover (FC), and forest edge length (FEL) on the occurrence of *Nyssorhynchus darlingi* **(A)** and *Nyssorhynchus albitarsis* s.l. **(B).** Internal nodes indicate data partitions and terminal nodes (bold boxes) show predicted mean abundance, sample size (*n*), and occurrence. Split points correspond to the variable and threshold maximizing variance reduction. Values are shown on the log scale for *Ny. albitarsis* s.l. and as predicted counts for *Ny. darlingi*.

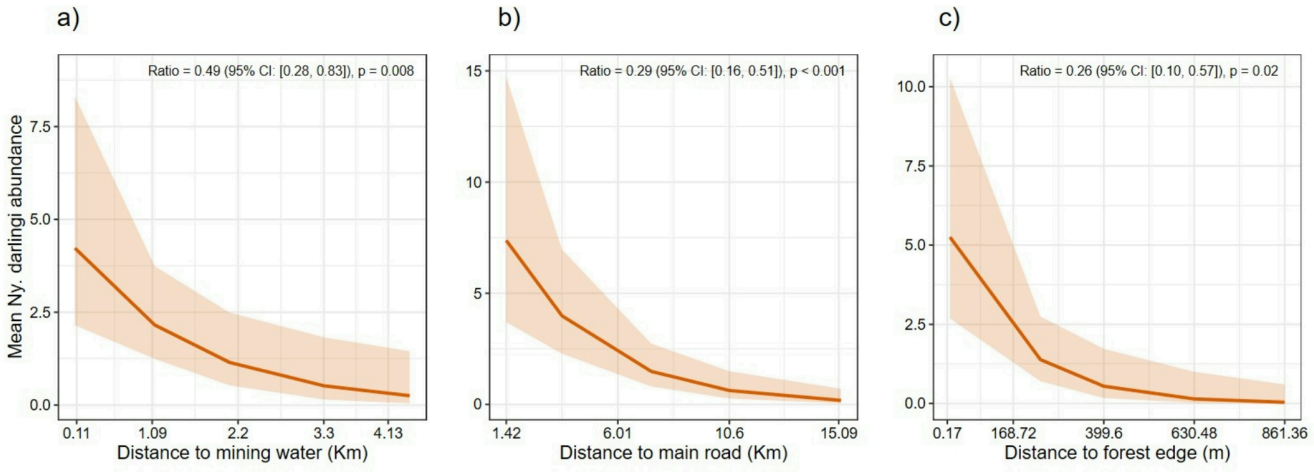


Figure 4

Local abundance of *Nyssorhynchus darlingi* in relation to landscape features across the mining gradient. The best-fitting GLMM (Group IV only) identified distance to mining water bodies **(A)**, main roads **(B)**, and forest edges **(C)** as significant predictors. Solid lines and shaded bands represent mean predictions and 95% confidence intervals (*CI*s). Effects are expressed as incidence rate ratios (IRRs) with 95% *CI*s shown within panels. Models assumed a Poisson distribution without overdispersion. Variables were fitted on a scaled basis, but x-axes are presented on the original scale.

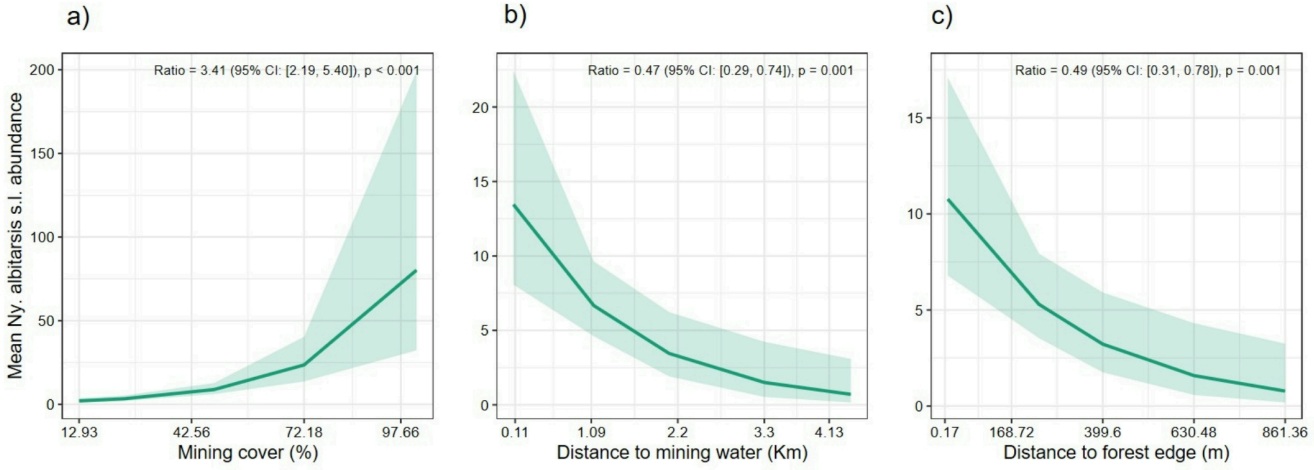


Figure 5

Local abundance of *Nyssorhynchus albitarsis* s.l. in relation to landscape features across the mining gradient. The best-fitting GLMM (Group IV only) identified mining cover **(A)**, distance to mining water

bodies **(B)**, and distance to forest edges **(C)**as significant predictors. Solid lines and shaded bands represent mean predictions and 95% confidence intervals (*CI*s). Effects are expressed as incidence rate ratios (IRRs) with 95% *CI*s shown within panels. Models assumed a Poisson distribution without overdispersion. Variables were fitted on a scaled basis, but x-axes are presented on the original scale.

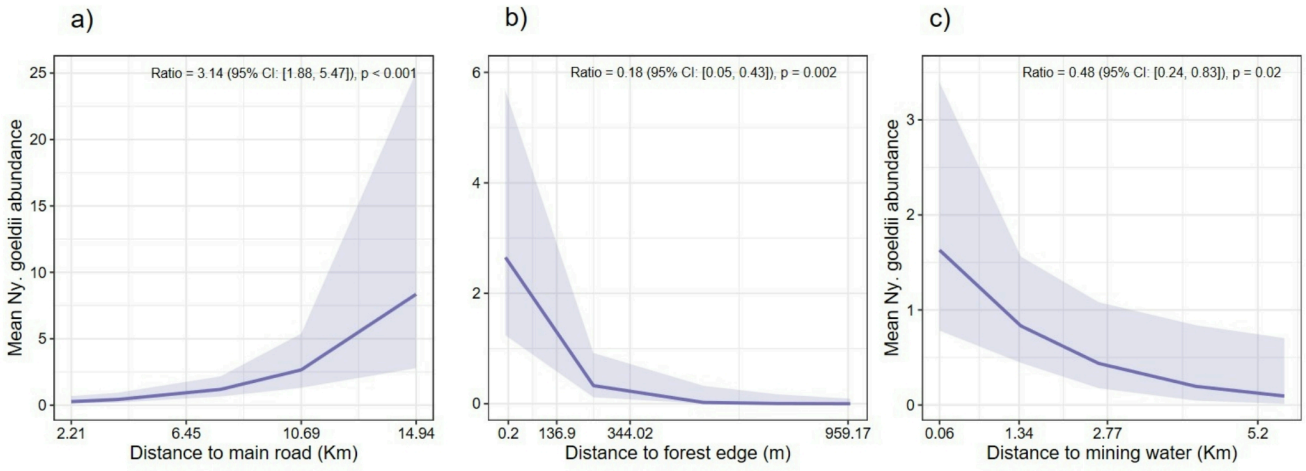


Figure 6

Local abundance of *Nyssorhynchus goeldii*in relation to landscape features across the mining gradient. The best-fitting GLMM (Groups III and IV) identified distance to main roads **(A)**, distance to forest edges **(B)**, and distance to mining water bodies **(C)** as significant predictors. Solid lines and shaded bands represent mean predictions and 95% confidence intervals (*CI*s). Effects are expressed as incidence rate ratios (IRRs) with 95% *CI*s shown within panels. Models assumed a Poisson distribution without overdispersion. Due to data sparsity, CIs were estimated using parametric bootstrap methods. Variables were fitted on a scaled basis, but x-axes are presented on the original scale.

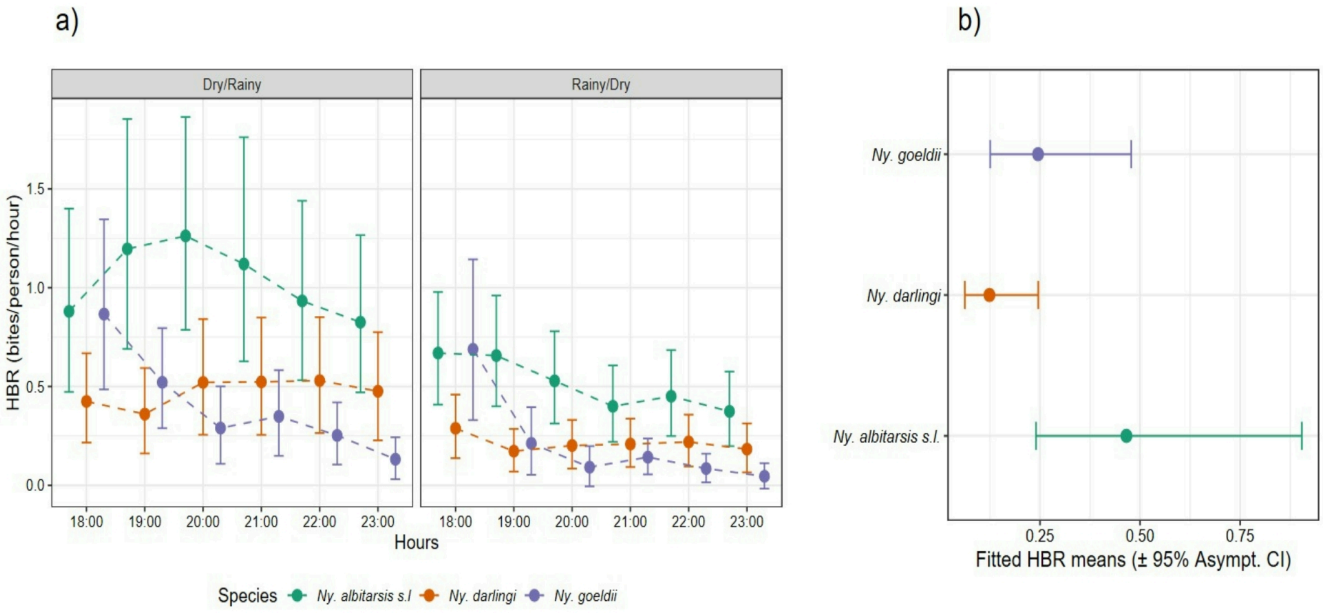


Figure 7

(A) Mean hourly human biting patterns (±95% *CI*) of *Nyssorhynchus albitarsis* s.l., *Ny. darlingi*, and *Ny. goeldii*, calculated from 6-h collections across localities and collection sites, over two sampling days during the Dry/Rainy and Rainy/Dry periods (pooled data). **(B)**Species effect on biting density estimated by a GLMM (mean Human Biting Rate estimates with 95% asymptotic confidence intervals), comparing the three mosquito species.

Supplementary Files

This is a list of supplementary files associated with this preprint. Click to download.

- SupplementaryInformationGrilletetal.2026.pdf